AFRL-RB-WP-TP-2010-3024

FEEDBACK FLOW CONTROL FOR A PITCHING TURRET (PART II) (POSTPRINT)

T. Vaithianathan and H.A. Carlson

Clear Science Corp.

R.D. Wallace, P.R. Shea, and M.N. Glauser

Syracuse University

JANUARY 2010

AIR FORCE RESEARCH LABORATORY
AIR VEHICLES DIRECTORATE
WRIGHT-PATTERSON AIR FORCE BASE, OH 45433-7542
AIR FORCE MATERIEL COMMAND
UNITED STATES AIR FORCE

REPORT DOCUMENTATION PAGE

Form Approved
OMB No. 0704-0188

1. REPORT DATE *(DD-MM-YY)*	2. REPORT TYPE	3. DATES COVERED *(From - To)*
January 2010	Conference Paper Postprint	07 April 2008 – 23 November 2009

4. TITLE AND SUBTITLE
FEEDBACK FLOW CONTROL FOR A PITCHING TURRET (PART II) (POSTPRINT)

5a. CONTRACT NUMBER
FA8650-08-C-3827

5b. GRANT NUMBER

5c. PROGRAM ELEMENT NUMBER
0605502

6. AUTHOR(S)
T. Vaithianathan and H.A. Carlson (Clear Science Corp.)
R.D. Wallace, P.R. Shea, and M.N. Glauser (Syracuse University)

5d. PROJECT NUMBER
A0DX

5e. TASK NUMBER

5f. WORK UNIT NUMBER
0C

7. PERFORMING ORGANIZATION NAME(S) AND ADDRESS(ES)

Clear Science Corp.
663 Owego Hill Road
Harford, NY 13784-0233

Syracuse University
Department of Mechanical and Aerospace Engineering
223 Link Hall
Syracuse, NY 13244

8. PERFORMING ORGANIZATION REPORT NUMBER

9. SPONSORING/MONITORING AGENCY NAME(S) AND ADDRESS(ES)
Air Force Research Laboratory
Air Vehicles Directorate
Wright-Patterson Air Force Base, OH 45433-7542
Air Force Materiel Command
United States Air Force

10. SPONSORING/MONITORING AGENCY ACRONYM(S)
AFRL/RBCA

11. SPONSORING/MONITORING AGENCY REPORT NUMBER(S)
AFRL-RB-WP-TP-2010-3024

12. DISTRIBUTION/AVAILABILITY STATEMENT
Approved for public release; distribution unlimited.

13. SUPPLEMENTARY NOTES
Conference presentation published in the Proceedings of the 48th AIAA Aerospace Sciences Meeting Including the New Horizons Forum and Aerospace Exposition, 4 - 7 January 2010, Orlando, FL. PAO Case Number: 88ABW-2009-5010; Clearance Date: 02 Dec 2009. Paper contains color.

14. ABSTRACT
Closed-loop systems have been developed for controlling the flow above a three-dimensional turret. The top of the turret is hemispherical, houses a flat optical aperture, and can rotate about two axes (pitch and yaw). The extent of separation and concomitant turbulence levels in the flow above the aperture change as the turret rotates. Suction jet slots circumscribing the aperture serve as control input; an array of pressure sensors on the turret surface provides the controller with information about the state of the flow above the surface. The control objective is to minimize the separation and turbulence in the dynamic environment created by the articulating turret. The closed-loop control systems include dynamical and measurement-based estimators, regulators, filters, and compensators. These components are developed using both computational and experimental data, and the control systems are evaluated through a series of control-in-the-loop CFD simulations and wind tunnel runs. Controller designs and computational tests are described in "Feedback Flow Control for a Pitching Turret (Part I), and the follow-on wind tunnel tests are described here.

15. SUBJECT TERMS
aerodynamic flow control, feedback flow control, turret, feedback control, separation control

16. SECURITY CLASSIFICATION OF:			17. LIMITATION OF ABSTRACT:	18. NUMBER OF PAGES	19a. NAME OF RESPONSIBLE PERSON (Monitor)
a. REPORT	b. ABSTRACT	c. THIS PAGE			James H. Myatt
Unclassified	Unclassified	Unclassified	SAR	20	19b. TELEPHONE NUMBER *(Include Area Code)* N/A

Standard Form 298 (Rev. 8-98)
Prescribed by ANSI Std. Z39-18

48th AIAA Aerospace Sciences Meeting Including the New Horizons Forum and Aerospace Exposition
4 - 7 January 2010, Orlando, Florida
AIAA 2010-361

Feedback Flow Control for a Pitching Turret (Part II)

R. D. Wallace,* P. R. Shea,* and M. N. Glauser †
Syracuse University, Syracuse, NY, USA
T. Vaithianathan ‡ and H. A. Carlson §
Clear Science Corp., Harford, NY, USA

Closed-loop systems have been developed for controlling the flow above a three-dimensional turret. The top of the turret is hemispherical, houses a flat optical aperture, and can rotate about two axes (pitch and yaw). The extent of separation and concomitant turbulence levels in the flow above the aperture change as the turret rotates. Suction jet slots circumscribing the aperture serve as control input; an array of pressure sensors on the turret surface provides the controller with information about the state of the flow above the surface. The control objective is to minimize the separation and turbulence in the dynamic environment created by the articulating turret. The closed-loop control systems include dynamical and measurement-based estimators, regulators, filters, and compensators. These components are developed using both computational and experimental data, and the control systems are evaluated through a series of control-in-the-loop CFD simulations and wind tunnel runs. Controller designs and computational tests are described in "Feedback Flow Control for a Pitching Turret (Part I), and the follow-on wind tunnel tests are described here.

I. Introduction

Turbulence, random density fluctuations, and aero-optical distortion in the flow around a turret can degrade the performance of a laser system housed within the turret. Laser light passing through the turbulent region is refracted by variations in density and optical path differences, scattering the light and reducing the laser intensity. One solution to the problem is to adapt the optical system in a way that compensates for the flow distortion—without altering the flow itself; for example, a morphing lens that keeps the laser focused in the presence of aero-optic distortions through contortions of the deformable mirror.[1] Another solution is to control (minimize)—either actively or passively—the flow fluctuations that cause aero-optical distortion.

In a passive flow control experiment, vortex generators mounted on the upstream side of a two-dimensional turret successfully reduced distortions at certain aperture angles of attack.[2] In another experiment, a spanwise array of synthetic jet actuators actively reduced flow fluctuations and delayed separation on a three-dimensional turret.[3] In an open-loop control experiment, synthetic jets were used to reduce the root-mean-square (rms) values of fluctuating velocity in the turbulent flow around a three-dimensional turret.[4]

Closed-loop control systems are designed to improve performance over open-loop systems through robustness, the ability to compensate for uncertainties over a range of flight conditions, and by achieving more with less—reducing actuator power, size, and weight requirements. A closed-loop system utilized synthetic jets to delay the onset of stall on a NACA 4412 airfoil, consuming less power than an open-loop system that increased stall angle by the same amount.[5,6] More recently, a proportional feedback controller was used to modulate synthetic jets on a 3D turret and reduce fluctuation levels in the wake.[7] The tests were performed at Mach 0.3 in the Subsonic Aerodynamic Research Laboratory (SARL) wind tunnel at Wright-Patterson Air Force Base, OH.

*Graduate Student, Syracuse University, Dept. Mech. & Aero. Engr., Syracuse, NY 13244-1240, AIAA Student Member.
†Professor, Syracuse University, Dept. Mech., Aero. & Manuf. Engr., Syracuse, NY 13244-1240, AIAA Associate Fellow.
‡Research Scientist, Clear Science Corp., 663 Owego Hill Road, Harford, NY 13784-0233.
§President, Clear Science Corp., 663 Owego Hill Road, Harford, NY 13784-0233, AIAA Associate Fellow.

Here, closed-loop flow control tests have been performed with a 3D turret at Mach 0.1. Compressible effects are not present at this speed, but systems for controlling velocity fluctuations in incompressible flows will be effective in controlling density fluctuations at higher speeds because of the strong correlation between velocity and density fluctuations.[8] Both computational and experimental tests were performed. The controller designs and computational tests are described in "Feedback Flow Control for a Pitching Turret (Part I)." The follow-on experimental tests are described here.

II. Problem Description

The control problem involves fully turbulent, incompressible flow past a three-dimensional (3D) turret, and the control objective is to minimize levels of separation and velocity fluctuations above the aperture. Free stream conditions in the computational simulations and the wind tunnel conditions in the experiment are approximately equal. The nominal free stream Reynolds number based on the diameter of the turret is 450,000, and the free stream Mach number is 0.1. The computational model of the turret and the wind tunnel test article also match—with some differences in the details. The turret consists of a six-inch-diameter hemisphere mounted on a six-inch-diameter cylinder. The cylinder is four inches in height. A flat aperture, 2.8 inches in diameter, is located at the top of the turret. The top, hemispherical section can rotate within the cylindrical stand in two directions: pitch and yaw. Rotation about the pitch axis alone is examined here.

The pitch angle is defined as the angle between a vector normal to the aperture and the free stream vector. When the normal is aligned with the turret centerline, the pitch angle is 90°. As the flat aperture pitches back, it becomes a backward facing ramp, separation levels increase as the pitch angle increases, and this increases levels of velocity fluctuations in the flow above and downstream of the aperture. The objective is to manage and minimize the separation and concomitant fluctuations in the aperture field of view as the pitch angle is varied sinusoidally.

Control-in-the-loop CFD simulations were used to develop and evaluate control designs and methods that are then applied in the wind tunnel. The CFD and wind tunnel controllers are comprised of the same components (described in "Feedback Flow Control for a Pitching Turret (Part I)"); however, these components are calibrated with CFD data for the control simulations and are calibrated with experimental data for the control tests in the wind tunnel. The intent is not to use experimental data to validate CFD models and methods but rather to develop and evaluate closed-loop control designs for the wind tunnel through CFD simulations.

III. The Experimental Test Configuration

The test facility at Syracuse University is a Gottingen-type, closed, recirculating tunnel in a horizontal configuration with continuously variable speeds of less than 4 m/s to approximately 70 m/s. The test section is constructed of optical Plexiglas with dimensions of 61 cm (width) x 61 cm (height) x 2.4 m (length). The turret is mounted directly to the floor of the tunnel. The left panel of Figure 1 contains a photograph of the test article, and the right panel contains a schematic of the top of the test article. Two concentric rings of suction jet slots circumscribe the aperture. Slots on one side of the centerplane are tied to a common manifold, and slots on the other to another manifold. Each manifold is connected to a vacuum system with a valve located between it and the slots. A total of 30 pressure sensors are located on and around the aperture. Surface pressures are sampled at a rate of 10 kHz using a NATIONAL INSTRUMENTS PXI-based 800 MHz signal conditioner with 24-bit, high-resolution A/D converters and anti-aliasing filter..

Suction jet velocity is controlled by cycling the suction valves at 25 Hertz and modulating the duty cycle. Velocity measurements were taken just above the slots using a hot wire probe to determine the relationship between suction velocity and duty cycle. From the left panel of Figure 2, the relationship is approximately linear between duty cycles of 30% and 90%. The right panel of Figure 2 contains a schematic of the Particle Imaging Velocimetry (PIV) system that is used to measure velocity in the flow. The DANTEC PIV System measures two components of velocity in the centerplane at a rate of 4 kHz using a DANTEC FLOWMAP system. The velocity measurements, surface pressure measurements, and suction valve duty cycle are phase aligned or synchronized in time.

Figure 3 contains photos of the mechanism that effects rotation about the pitch and yaw axes, housed under the top of the turret. A drive shaft connects a stepper motor to the turret top through a gearing system, generating rotation about the pitch axis. Another stepper motor generates yaw rotation. The motors

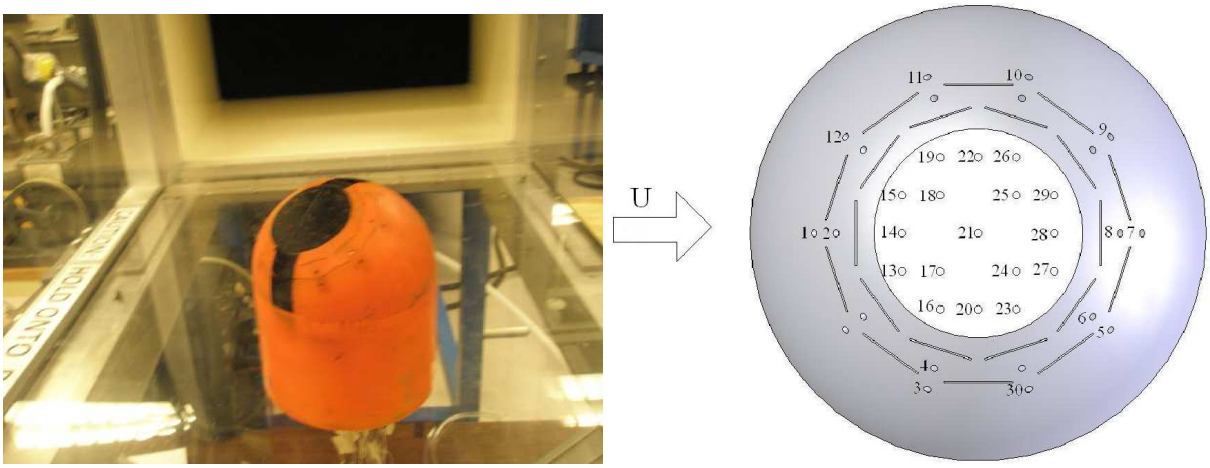

Figure 1. The test article (left) and a schematic of the top of the turret with sensor and actuator arrays(right). Jet slots are marked as lines and sensors as open circles.

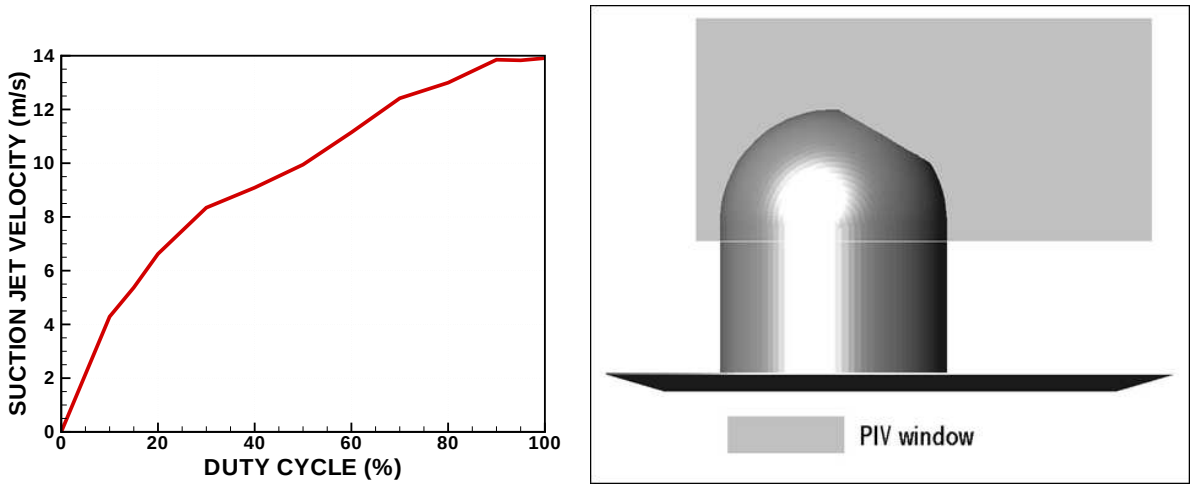

Figure 2. Suction jet velocity versus suction valve duty cycle (left) and a schematic of the PIV window (right).

are rated to 58.61 Newton-cm of torque and are controlled by the data acquisition system, LabVIEW.

IV. Static and Dynamic Pitching

The first series of wind tunnel tests examine pitch angles between 110° and 120°. These tests were conducted with no actuation and with constant actuation at 30%, 50%, 70%, and 90% duty cycles (open loop). The turret is stationary at each individual pitch angle in a set of static runs, and the turret rotates over the pitch angle range in dynamic tests. The intent is to examine the effect of the turret motion on the flow. Velocity is sampled at 4 Hertz and surface pressures at 10 kilo-Hertz. The top panels of Figure 4 contain contours and streamlines of time-averaged velocity in the PIV centerplane at static pitch angles of 115° and 120° (with no actuation). In both cases, the flow is—on average—fully separated in the region above the aperture. The pitch angle of 115° marks the point of incipient separation with a stationary turret: flow was separated above the aperture in one run at this angle and attached in another. The flow was always attached at lower static angles and always separated at higher angles. The bottom panels of Figure 4 contain time histories of surface pressure from five sensors located on the turret centerline: Sensor Nos. 1, 14, 21, 28, and 7 (see the sensor locations in the right panel of Figure 1).

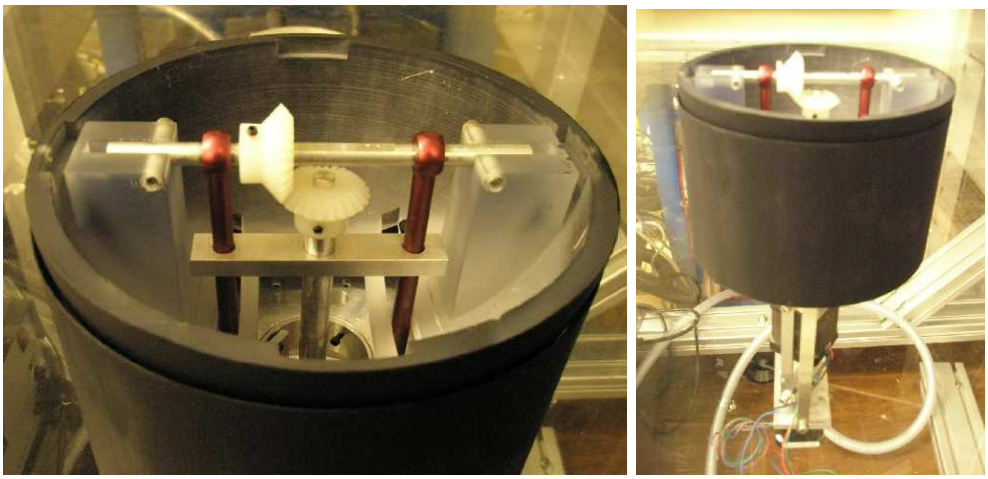

Figure 3. Photos of the two-degree-of-freedom rotational mechanism housed inside the turret.

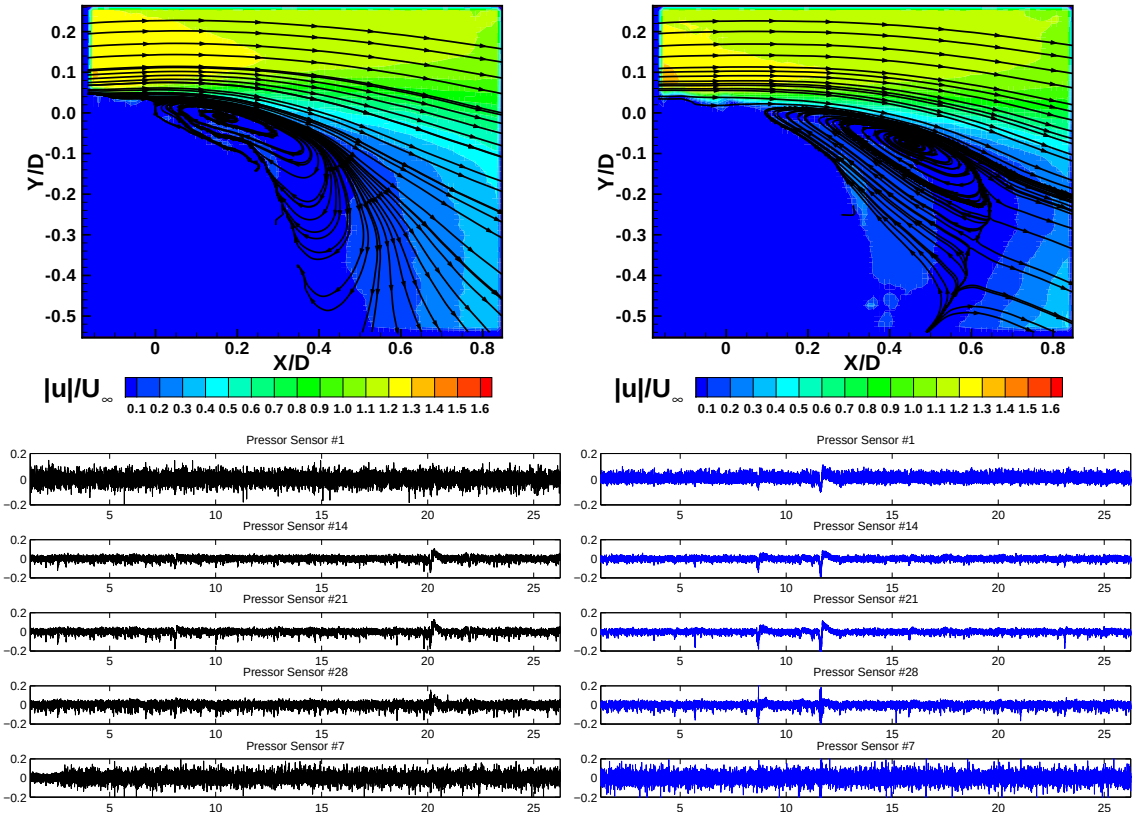

Figure 4. Contours and streamlines of time-averaged velocity on the PIV centerplane (top panels) and time histories of surface pressure from five sensors located on the turret centerline (bottom panels) at static pitch angles of 115° **(left) and** 120° **(right) with no suction jet actuation.**

Next, the turret pitches dynamically over a range from 110° to 120° using the following prescribed function:

$$\theta(t) = [115 - 5\cos(\omega t)]\,\tfrac{\pi}{180} \tag{1}$$

where $\omega = d\theta/dt = 6\pi/25$ rad/s. Therefore, one pitching period is $8\frac{1}{3}$ seconds. Again, velocity is sampled at 4 Hertz and pressure at 10 kilo-Hertz.

Figure 5 contains results from the dynamic run with no actuation. The data has been ensemble averaged over a number of pitching cycles. Comparing the top and bottom panels on the left, the flow is attached as the pitch angle increases through 115° and detached as it decreases through 115°. In fact, when the angle is increasing, the flow remains attached until 119°—at which point, it becomes massively separated. As the angle reaches the maximum of 120° and begins to decrease, the flow remains separated until 112° when it re-attaches. The bottom right panel of Figure 5 contains time histories of surface pressure from Sensor Nos. 1, 14, 21, 28, and 7. The fluctuating pressure ahead of the aperture (Sensor No. 1 in the topmost time series) increases as turret pitches back and the flow separates. However, the sensors located on and downstream of the aperture (Sensor Nos. 14, 21, 28, and 7 in the lower four time series) exhibit an opposite trend: fluctuating pressures *decrease* as the flow separates. Comparing results from the static and dynamic runs reveals that the influence of dynamic rotation is significant even when the pitching rate is modest.

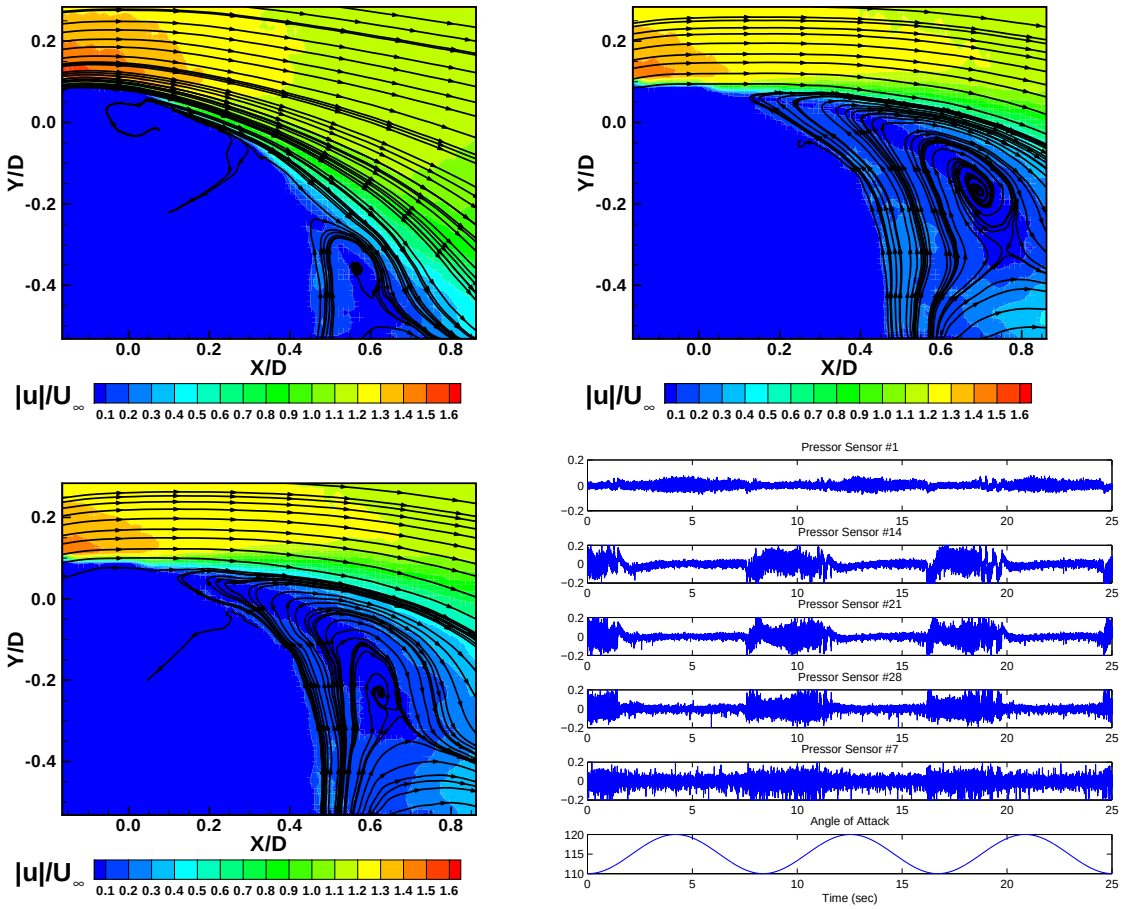

Figure 5. Velocity contours and streamlines in the PIV centerplane from the run with dynamic pitching and no actuation at dynamic pitch angles of 115° (increasing) in the top left panel, 120° in the top right panel, and 115° (decreasing) in the bottom left panel. Time histories of five surface pressures on the turret centerline from the dynamic run in the bottom right panel.

Open-loop flow control runs were executed with a pitching turret and steady suction at 30%, 50%, 70%, and 90% duty cycles. Figure 6 contains results from the dynamic run at 50% duty cycle. Again, the data are ensemble averaged over a number of pitching cycles. From the panels containing velocity contours and streamlines, steady suction at the 50%-duty-cycle level moves the separated flow downstream and below the aperture. Comparing the bottom right panels of Figures 5 and 6, steady suction—and the elimination of separation above the aperture that results—actually increases pressure fluctuations in all but one of the sensors. Assuming that separation promotes turbulent fluctuations in the flow, the only sensor that follows the expected trend is Sensor No. 1. It is also the only sensor located upstream of the jet slots. Root-mean-square values of fluctuating surface pressures are higher than baseline values in all of the open-loop runs (for all of the sensors but Sensor No. 1). The same trend was confirmed at a duty cycle of 100% (valves fully

open)—eliminating transmission of vibrations from the valves as a possible source of the trend.

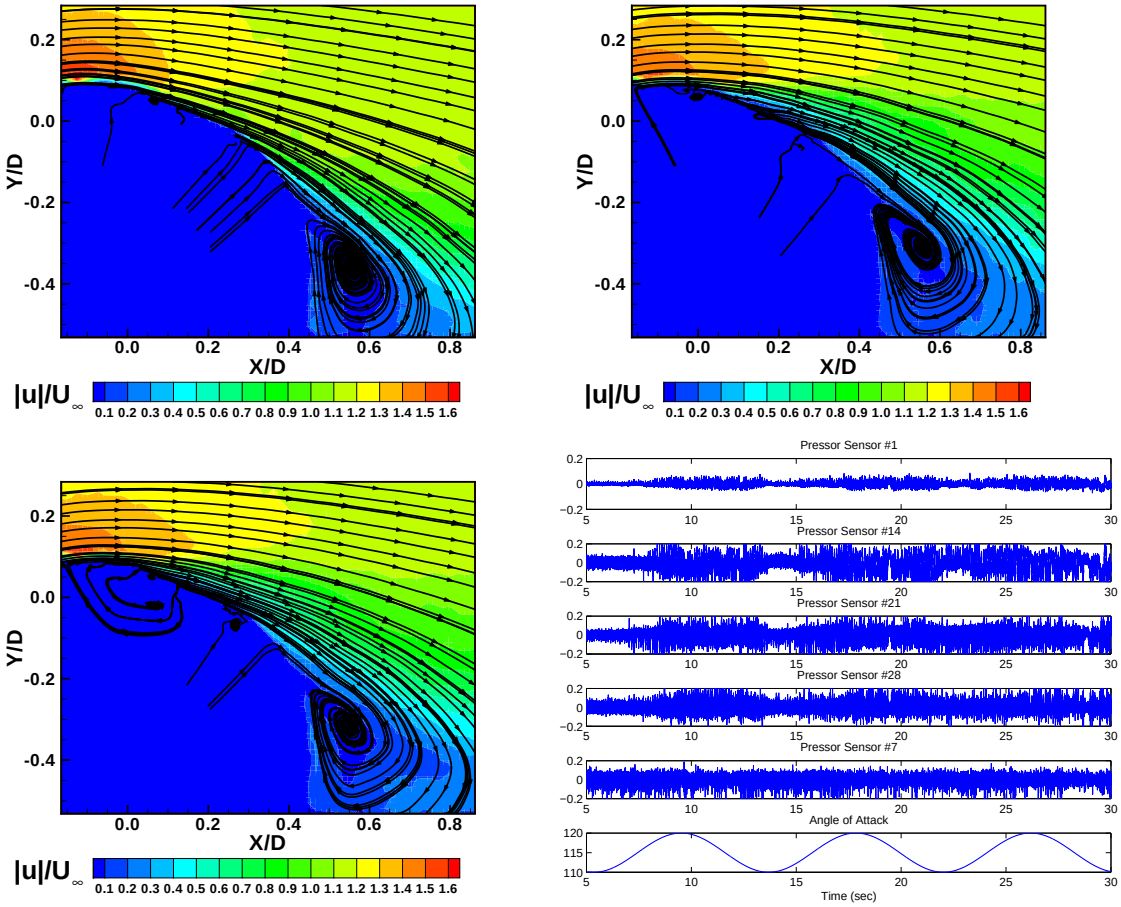

Figure 6. Velocity contours and streamlines in the PIV centerplane from the run with dynamic pitching and open-loop control (50% duty cycle) at dynamic pitch angles of 115° **(increasing) in the top left panel,** 120° **in the top right panel, and** 115° **(decreasing) in the bottom left panel. Time histories of five surface pressures on the turret centerline from the dynamic run in the bottom right panel.**

V. Initial Closed-loop Control Run

The initial closed-loop control run in the wind tunnel utilized a single pressure sensor (Sensor No. 1), chosen because its rms values decrease as duty cycle increases in the open-loop tests. A simple proportional controller was employed in the initial test. The control objective is to minimize fluctuations in the single-sensor pressure measurement, using suction. The duty cycle of the suction valve is modulated by the controller. The turret pitches at a maximum rate of 3.768 degrees per second between 110° and 120° according to the function in (1). One pitching period is $8\frac{1}{3}$ seconds. Velocity is sampled at 4 Hertz for a total of 102 pitching cycles (850 seconds), yielding 3400 PIV snapshots. This corresponds to 100 snapshots over every three pitching cycles, and PIV data are distilled by averaging values from 34 three-cycle periods. Pressure is sampled at 10 kilo-Hertz. All of the 20 jet slots were activated, operating as a single unit.

Four control runs were executed, using four different types of pressure filters:

- Band Pass: Frequencies (Hz) in the range $[30, 500]$
- Band Stop: Frequencies (Hz) in the range $[0, 8] \cup [12, 500]$.
- Low Pass: Frequencies (Hz) in the range $[0, 500]$.
- Very Low Pass: Frequencies (Hz) in the range $[0, 8]$.

Performance output is defined as

$$u_{\mathrm{rms}}(t) \equiv \sqrt{\frac{1}{N_{\mathrm{PIV}}}\left(\sum_{i=1}^{N_{\mathrm{PIV}}}\{[u_1(\boldsymbol{x}_i,t)-\bar{u}_1(\boldsymbol{x}_i)]^2+[u_2(\boldsymbol{x}_i,t)-\bar{u}_2(\boldsymbol{x}_i)]^2\}\right)} \tag{2}$$

where $u_{1,2}(\boldsymbol{x}_i,t)$ are the instantaneous velocities in the centerplane, and $\bar{u}_{1,2}(\boldsymbol{x}_i)$ are the mean (time-averaged) velocities. N_{PIV} is the number of PIV-sampled points on the centerplane.

The results are summarized in Table 1. The column labeled "$\langle DC\rangle$ (%)" contains time-averaged values of the jet duty cycle. Values in the rightmost column are measures of control effectiveness or efficiency (the ratio of fluctuating velocity reduction to required control input):

$$\xi = \left|\frac{\langle u_{\mathrm{rms}}\rangle_{\mathrm{Control}} - \langle u_{\mathrm{rms}}\rangle_{\mathrm{No\ Control}}}{\langle DC\rangle}\right|. \tag{3}$$

Higher values of ξ correspond to more efficient controllers. Two of the simple closed-loop controllers reduce velocity fluctuations more than the representative open-loop case (50% duty cycle). Based on the ratio ξ in the rightmost column of the table, all of the closed-loop controllers operate more efficiently than the open-loop system. The runs with the band-pass and low-pass filters perform most efficiently, and data from the run with the band-pass filter are used to construct an advanced controller.

Run Description	$\langle u_{\mathrm{rms}}\rangle$	$\langle DC\rangle$ (%)	ξ
No Control	9.65	–	–
Open-loop Control	4.14	50	0.11
Closed-loop Control (Band Pass)	4.67	33	0.15
Closed-loop Control (Band Stop)	3.86	44	0.13
Closed-loop Control (Low Pass)	3.47	42	0.15
Closed-loop Control (Very Low Pass)	5.14	35	0.13

Table 1. Summary of results from the wind tunnel runs. ξ is defined in (3) and is a measure of controller efficiency.

Figure 7 compares results from the band-pass-filtered closed-loop run, an open-loop run, and the baseline run with no control jets: time histories of performance output (rms values of fluctuating velocity and control input (jet momentum coefficient). From the top right, top left, and bottom right panels of Figure 8, the separation region is moved aft of and below the aperture by the initial closed-loop controller as it was by the open-loop controller.

VI. Controller Design

Next, data from the initial closed-loop run are used to construct an advanced controller. The advanced controller is designed in Clear Science Corp.'s software, SMARTFLOW, as described in the companion paper, "Feedback Flow Control for a Pitching Turret (Part I)." The control objective in the initial runs was to minimize pressure fluctuations from the single pressure sensor, but the true objective is to minimize velocity fluctuations (u_{rms}) in a portion of the aperture field of view close to the aperture surface. The actual field of view is three dimensional, but the PIV window intersects this volume on the turret centerplane. PIV measurements are used to construct the estimators. They are not available to the controller in real time but are used to evaluate controller performance.

The single pressure sensor used in the initial closed-loop runs was chosen because it correlated well with pitch angle: pressure variance increased as the angle (and extent of flow separation) increased. The correlation seems to be due primarily to the sensor's location upstream of the jet slots, which will change as the yaw angle changes. A more robust controller will utilize multiple sensors by relying on a general pressure-velocity correlation contained within the measurement-based estimator as described in "Feedback Flow Control for a Pitching Turret (Part I)"—rather than any specific relationship between surface pressures and velocity. The measurement-based estimator in the more advanced controller utilizes 18 sensors: Sensor

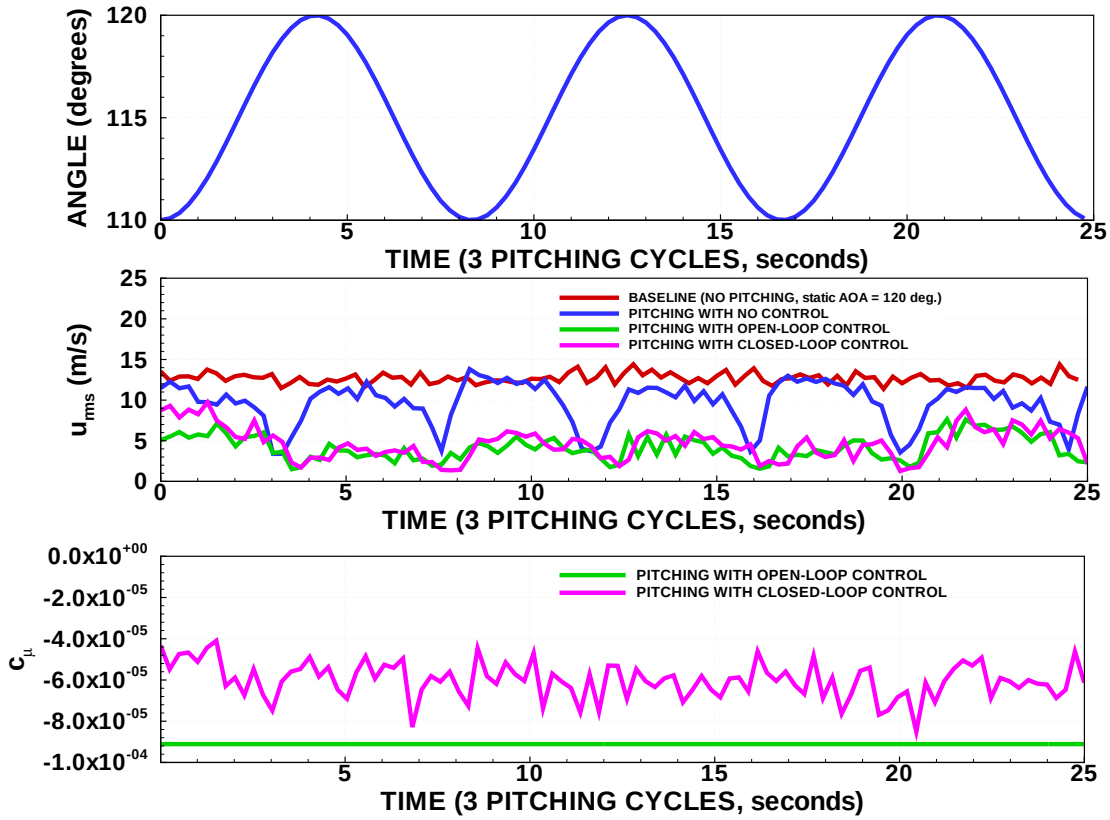

Figure 7. Comparisons of the baseline (no control), open-loop control, and initial closed-loop control runs.

Nos. 1, 2, 3, 5, 6, 8, 11, 12, 13, 14, 15, 16, 17, 18, 25, 26, 29 and 30, identified in the right panel of Figure 1. These sensors maximize the correlation between pressure and velocity. Pressure sensors are located on the aperture itself for the purpose of investigating the flows and developing preliminary controllers; however, these sensors would interfere with operation in real applications, and final designs would exclude them.

The first step in constructing estimators is to compute a set of POD basis functions using PIV snapshots. The left panel of Figure 9 contains the POD energy distributions in the reduced-order model (ROM) built with snapshots obtained from the initial closed-loop run. Four POD modes contain more than 80% of the perturbation energy, and this number of modes is chosen for the estimators. The right panel of Figure 9 contains comparisons of time histories of rms velocity fluctuations from the PIV data (labeled as "RAW") and time histories obtained by projecting the PIV snapshots onto the four POD modes: $u_{\rm rms}(t) \approx \sqrt{a_{(n)}(t) a_{(n)}(t)},\ n = 1, 4$. Even with only four modes in the models, the approximations based on projections are very accurate.

The next step is to use the POD models to construct the measurement-based and dynamical estimators described in "Feedback Flow Control for a Pitching Turret (Part I)"—both of them linear. Figure 10 contains time histories of the POD coefficients from the dynamical estimators (D-EST), the measurement-based estimators (M-EST), along with the values obtained by projecting the PIV snapshots onto the four POD modes. From the top left panel of the Figure 10, predictions from both types of estimator are accurate in predicting the trends in the first POD coefficient, and this mode contains more than 75% of the perturbation energy. Note how much less noise there is in the dynamical state estimates than in the measurement-based state estimates. This will be exploited with the Kalman filter.

Again, the control objective in the wind tunnel is to minimize velocity fluctuations in the aperture field of view (or at least over the area of intersection between the PIV window and field of view). Figure 11 contains approximations of $u_{\rm rms}$ from the dynamical and measurement-based estimators, along with values from the projected POD coefficients. From Figure 11, the dynamical estimator is able to accurately track the velocity

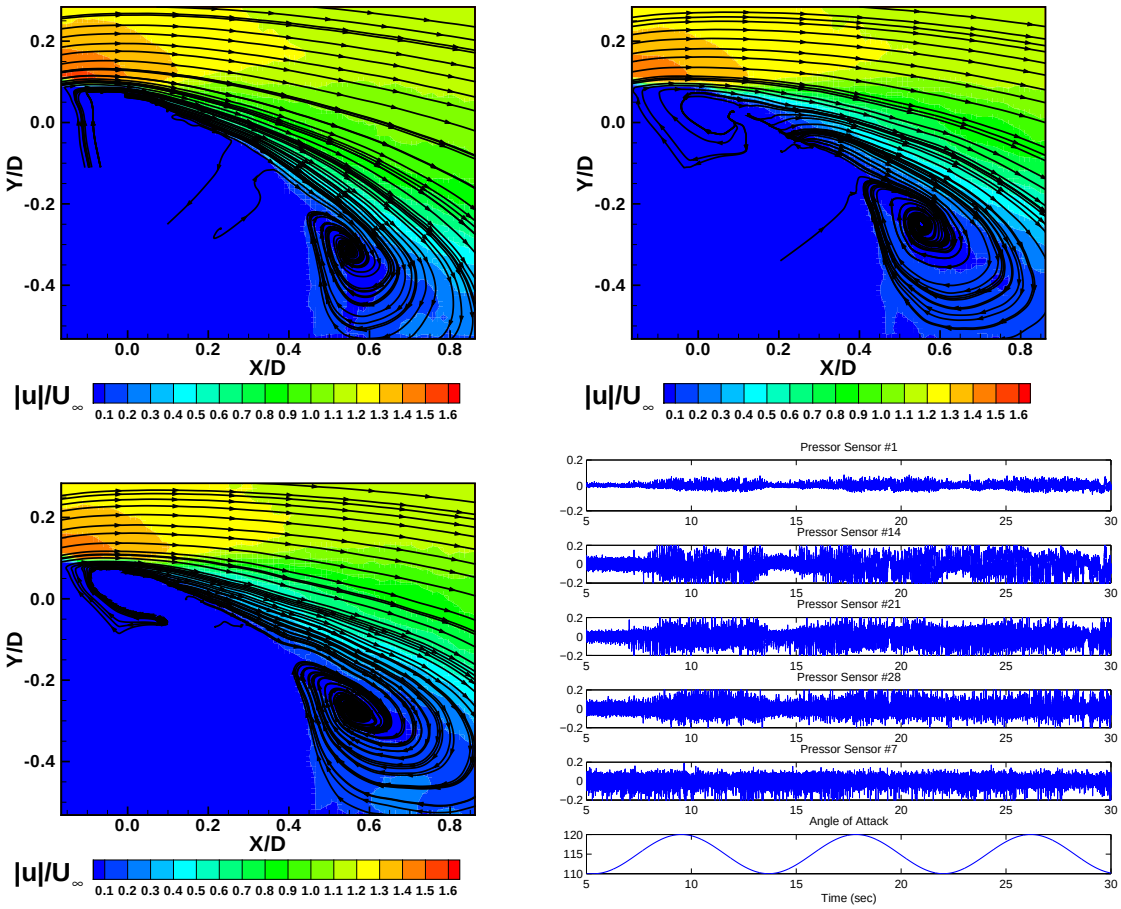

Figure 8. Velocity contours and streamlines in the PIV centerplane from the run with dynamic pitching and simple closed-loop control (Band-Pass) at dynamic pitch angles of 115° (increasing) in the top left panel, 120° in the top right panel, and 115° (decreasing) in the bottom left panel. Time histories of five surface pressures on the turret centerline from the dynamic run in the bottom right panel.

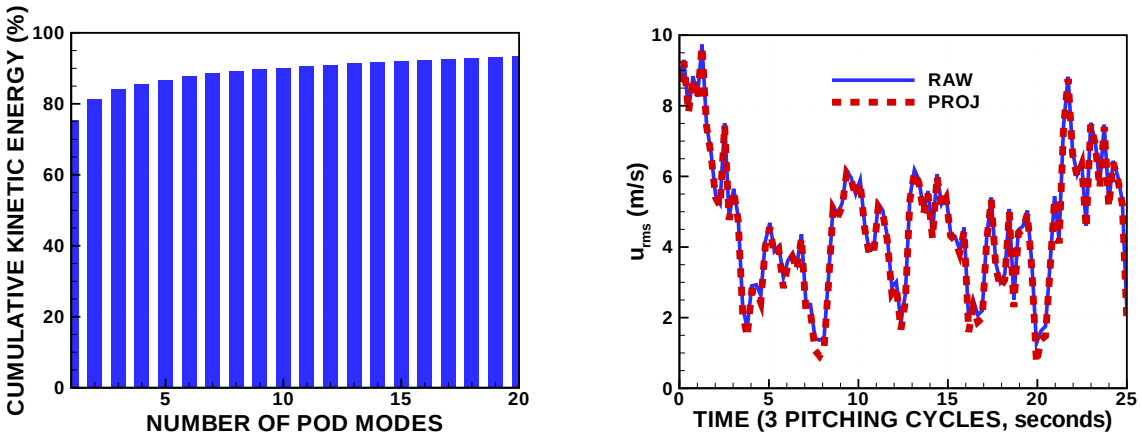

Figure 9. Energy distribution in the POD-based ROM (left). Time histories of u_{rms} from the PIV data (RAW) and approximations obtained by projecting the PIV snapshots onto the first four modes in the model (PROJ) (right).

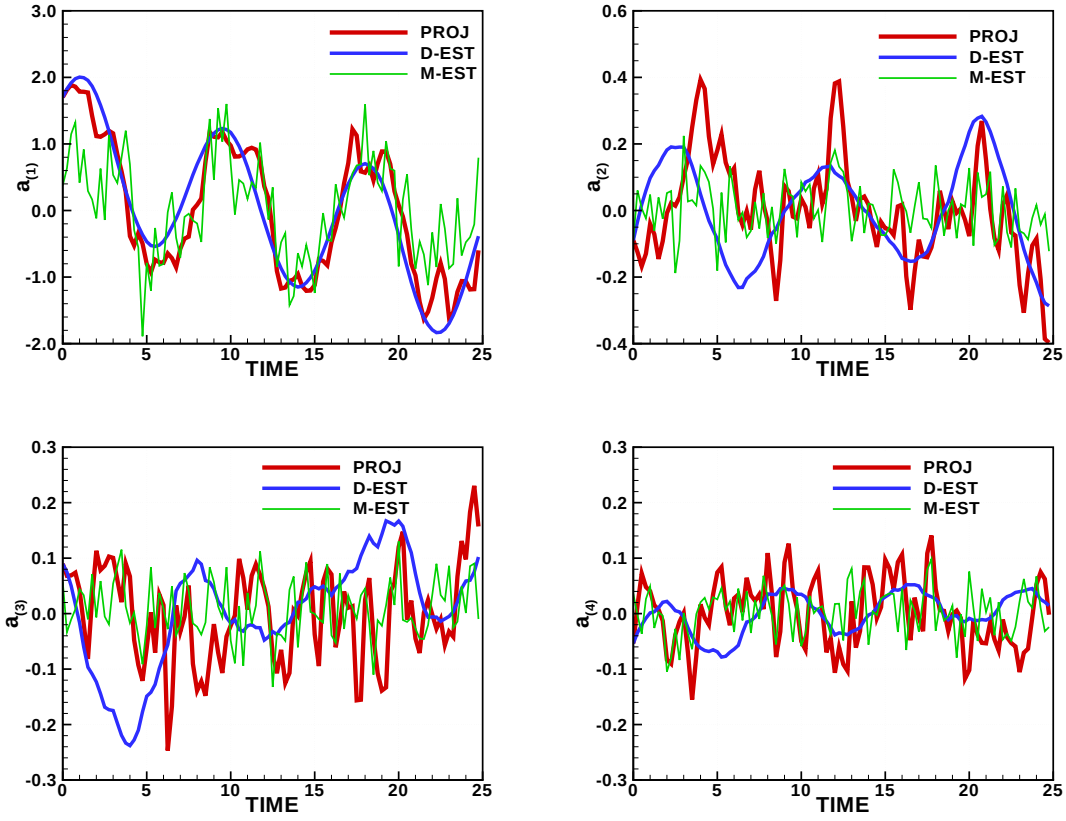

Figure 10. Time histories of the first four POD coefficients from the dynamical estimator (D-EST), the measurement-based estimator (M-EST), and values obtained by projecting the PIV snapshots onto the four POD modes of the model (PROJ).

fluctuations. The measurement-based estimator exhibits relatively high noise levels—even when the pressure signals are filtered—but the dynamical estimator and Kalman filter described in "Feedback Flow Control for a Pitching Turret (Part I)" are designed to address this issue.

With performance output defined as spatially integrated values of $u_{\mathrm{rms}}(t)$, the controller will utilize approximations from the estimators, and the PI regulator described in "Feedback Flow Control for a Pitching Turret (Part I)" becomes

$$\dot{u} = k_1(\sqrt{\hat{x}_n(t)\hat{x}_n(t)} - 0) + k_2 \int_0^t (\sqrt{\hat{x}_n(\tau)\hat{x}_n(\tau)} - 0)d\tau \tag{4}$$

where u is the suction valve duty cycle percentage and the objective is to reduce fluctuating velocity to zero. The gains ($k_{1,2}$) are determined heuristically, which can be a time-consuming process involving a number of wind tunnel runs. Alternatively, a Linear Quadratic Regulator (LQR) automatically determines gains that minimize the following cost function:

$$J \equiv \frac{1}{T} \int_0^T (\hat{x}_n \hat{x}_n + r\dot{u}^2)dt. \tag{5}$$

The parameter r weights the penalty assigned to the control input ($\dot{u}$).

Next, the dynamical estimator from "Feedback Flow Control for a Pitching Turret (Part I)" is written as

$$\dot{\hat{\boldsymbol{x}}} = \boldsymbol{a}_0 + \boldsymbol{A}_1\hat{\boldsymbol{x}} + \boldsymbol{b}_0 u + \boldsymbol{b}_2\dot{u} + \boldsymbol{C}\boldsymbol{w} \quad \text{and} \quad \dot{\boldsymbol{w}} = \boldsymbol{H}\boldsymbol{w} \tag{6}$$

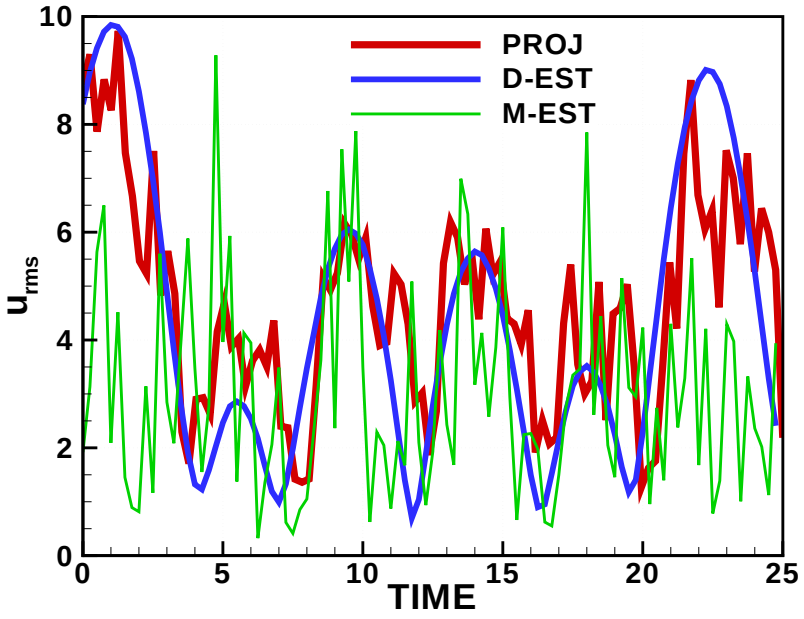

Figure 11. Approximations of $u_{\rm rms}$ from the dynamical estimators (D-EST), measurement estimators (M-EST), along with values obtained from projected POD coefficients (PROJ).

where

$$\boldsymbol{C} = (\boldsymbol{b}_3 \;\; \boldsymbol{b}_4), \quad \boldsymbol{w} = (\dot{\eta}, \ddot{\eta})^T, \quad \text{and} \quad \boldsymbol{H} = \begin{pmatrix} 0 & 1 \\ -\omega^2 & 0 \end{pmatrix}. \tag{7}$$

ω is the pitching frequency, defined in (1). Defining an augmented state estimate as $\boldsymbol{z} \equiv (\hat{\boldsymbol{x}}, u, \boldsymbol{w})^T$ and minimizing the cost function in (5) produces the following control law:

$$\dot{u} = -K_m^{LQR} z_m. \tag{8}$$

The dynamical estimator without the Kalman filter were imported from SMARTFLOW into Matlab, and the following gains were computed:

$$\boldsymbol{K}^{LQR} = (-0.2746 \;\; 0.5013 \;\; 0.0482 \;\; -0.0949 \;\; 0.0064 \;\; -1.3309 \;\; -3.2540)^T \times 10^3. \tag{9}$$

The gains in (9) were computed after reducing the weighting factor r in (5) to its lowest possible value, which effectively imposes no penalty on the control input.

VII. Closed-loop Control Run with an Advanced Controller

Three compensators (LQR regulators with Kalman filters) were designed using three different values of the process covariance. As the process covariance decreases, the controller relies more on the dynamical estimator and less on the measurement-based estimator—see "Feedback Control for a Pitching Turret (Part I)" for a definition of the term. From Table 2, the process covariance is highest in Run 1 and lowest in Run 3. Measurement error covariance is 3.3×10^{-4} in all three runs.

Figure 12 contains time histories of fluctuating velocity (middle panel) and jet momentum coefficient (bottom panel) from the three control runs, along with baseline histories from the uncontrolled run. Comparing the blue, pink, and red curves in the middle panel, it is clear that heavy reliance on the dynamical estimator results in poorer performance. The best control is achieved in Run 1 where the measurement-based estimator dominates. From the pink and red curves in the bottom panel of Figure 12, the Kalman filter

Quantity	Symbol	Run 1	Run 2	Run 3
Signal-to-Noise Ratio	SNR	5.0	5.0	5.0
Process covariance	W_p	3.3×10^{-1}	3.3×10^{-4}	3.3×10^{-7}
Measurement covariance	V_p	3.3×10^{-4}	3.3×10^{-4}	3.3×10^{-4}

Table 2. Parameter settings for the wind tunnel control runs.

reduces noise in the control input significantly when the dynamical estimator is heavily weighted; however, the blue curve indicates that substantial filtering is effected even in Run 1 when the dynamical estimator is weighted much less: compare the relatively smooth blue curve in the bottom panel of Figure 12 with the noisy pink curve in the bottom panel of Figure 7.

From the bottom panel of Figure 12, the control input modulates with pitch angle in all three runs with the advanced controllers. The phase shift between pitch angle and input varies between the three runs, but the turret motion is clearly driving the input, and modulation in the jet amplitude is not small. Conversely, the pink curve in the bottom panel of Figure 7 indicates little or no correlation between control input from the simpler controller and pitch angle: modulations in the jet momentum coefficient are essentially random.

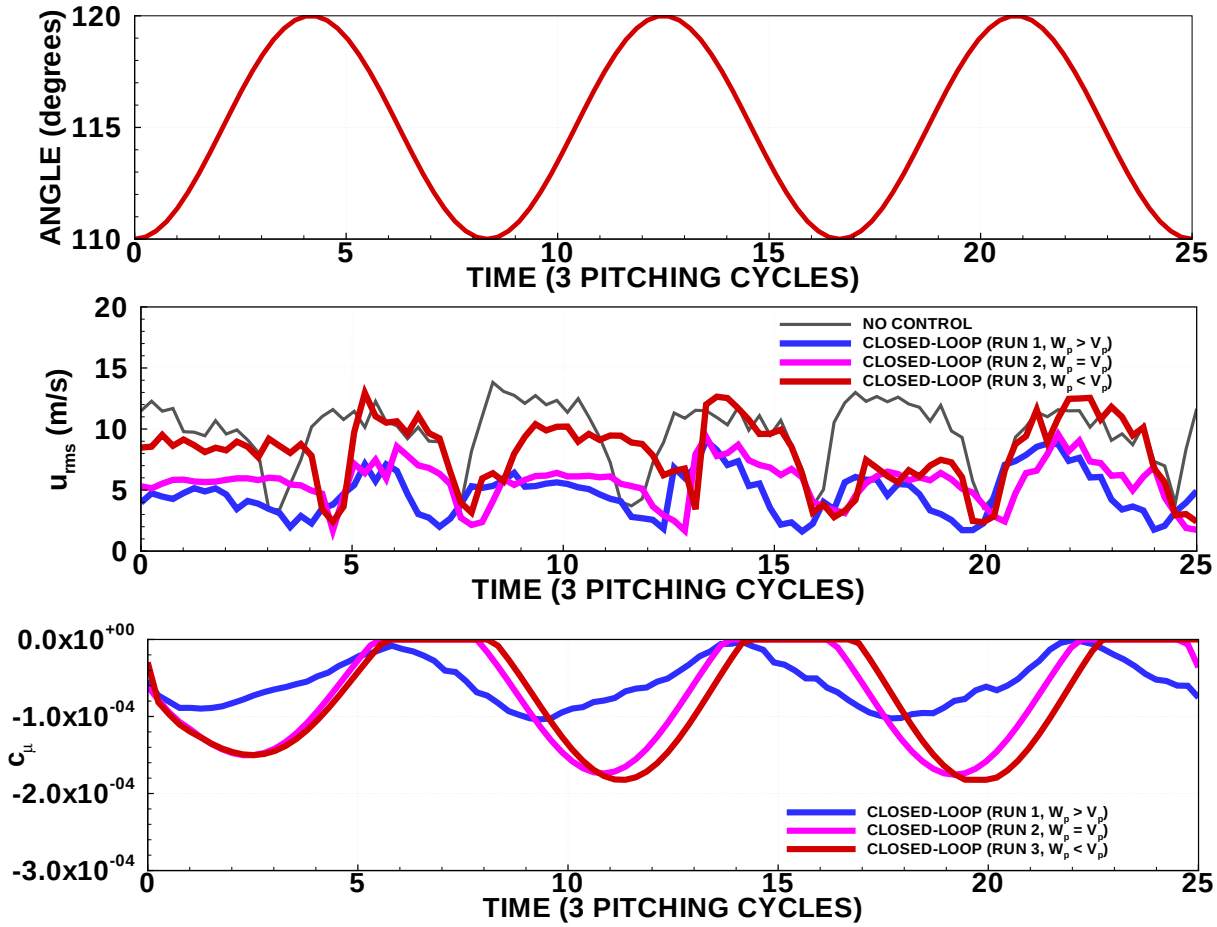

Figure 12. Comparison of pitching runs with and without control: results from the new controller.

Table 3 summarizes results from the various runs: time-averaged values of fluctuating velocity, control input ($\langle DC \rangle$), and controller efficiency (ξ)—defined in (3). Higher values of ξ correspond to more efficient controllers. Again, the run with a steady suction jet operating at 50% duty cycle is chosen as the

representative open-loop case. It effects the largest reduction in fluctuating velocity (57%); however, it is significantly less efficient than the two most efficient closed-loop controllers. The most efficient simple controller (band-pass) reduces fluctuating velocity by 52% and the most efficient advanced controller (Run 1) by 51%. Comparing the bottom left panels of Figures 6, 8, and 13, separated flow is, on average, closer to the aperture at a pitch angle of 115° (decreasing) in the advanced-controller run (Run 1) than it is in the open-loop and simple closed-loop control runs—reflecting the slightly higher time-averaged fluctuating velocity in the advanced-controller run. Comparing the bottom right panels of Figures 6, 8, and 13, the behavior of fluctuating pressures from the five sensors on the turret centerline is qualitatively similar in the open-loop, simple closed-loop, and advanced closed-loop runs. From the values of ξ in Table 3, the advanced controller in Run 1 is 13% more efficient than the most efficient simple controller and 55% more efficient than open-loop control.

Run Description	$\langle u_{\text{rms}} \rangle$	$\langle DC \rangle$ (%)	ξ
No Control	9.65	–	–
Open-loop Control	4.14	50	0.11
Simple Closed-loop Control (Band Pass)	4.67	33	0.15
Advanced Closed-loop Control (Run 1, $W_p > V_p$)	4.69	30	0.17
Advanced Closed-loop Control (Run 2, $W_p = V_p$)	5.64	40	0.10
Advanced Closed-loop Control (Run 3, $W_p < V_p$)	7.97	41	0.04

Table 3. Summary of results from the wind tunnel runs with open- and closed-loop control. ξ in the rightmost column is defined in (3) and is a measure of control efficiency—the ratio of fluctuating velocity reduction to required suction.

VIII. Conclusion

Closed-loop systems for controlling flow separation and turbulence above a pitching turret have been developed and tested through a series of control-in-the-loop CFD simulations and wind tunnel runs. The wind tunnel tests have been described here; controller designs and the computational tests are described in the companion paper, "Feedback Flow Control for a Pitching Turret (Part I)." Levels of flow separation and turbulence change as the turret pitches, and the systems successfully reduce these levels in the dynamic environment through feedback control—meeting the objective of control in the presence of disturbances over a range of operating conditions. Another objective is the minimization of control input: achieving threshold levels of control with less actuator energy. Closed-loop systems in the wind tunnel runs are as much as 55% more efficient than a representative open-loop system as measured by the ratio of reduction in fluctuating velocity to required control input.

Acknowledgments

This material is based upon work supported by the US Air Force Research Laboratory's Air Vehicles Directorate under Contract FA8650-08-C-3827. Any opinions, findings, conclusions, or recommendations expressed in the material are those of the authors and do not necessarily reflect the views of the US Air Force.

References

[1]A. M. Nightingale, B. Goodwine, M. Lemmon, and E. J. Jumper, "Feed-forward Adaptive-Optic System Identification Analysis for Mitigating Aero-Optic Disturbances," AIAA Paper 2007-4013, *38th AIAA Plasmadynamics and Lasers Conference*, Miami, FL, 2007.

[2]S. Gordeyev, T. E. Hayden, and E. J. Jumper, "Aero-Optical and Flow Measurements Over a Flat-Windowed Turret," *AIAA Journal*, Vol. 45, No. 2, 2007, pp. 347-357.

[3]B. Vukasinovic, and A. Glezer, "Control of a Separating Flow over a Turret," *37th AIAA Fluid Dynamics Conference*, AIAA Paper 2007-4506, Miami, Florida, 2007.

[4]M. Y. Andino, R. D. Wallace, R. F. Schmit, R. C. Camphouse, J. H. Myatt, and M. N. Glauser, "Flow and Aero-Optics

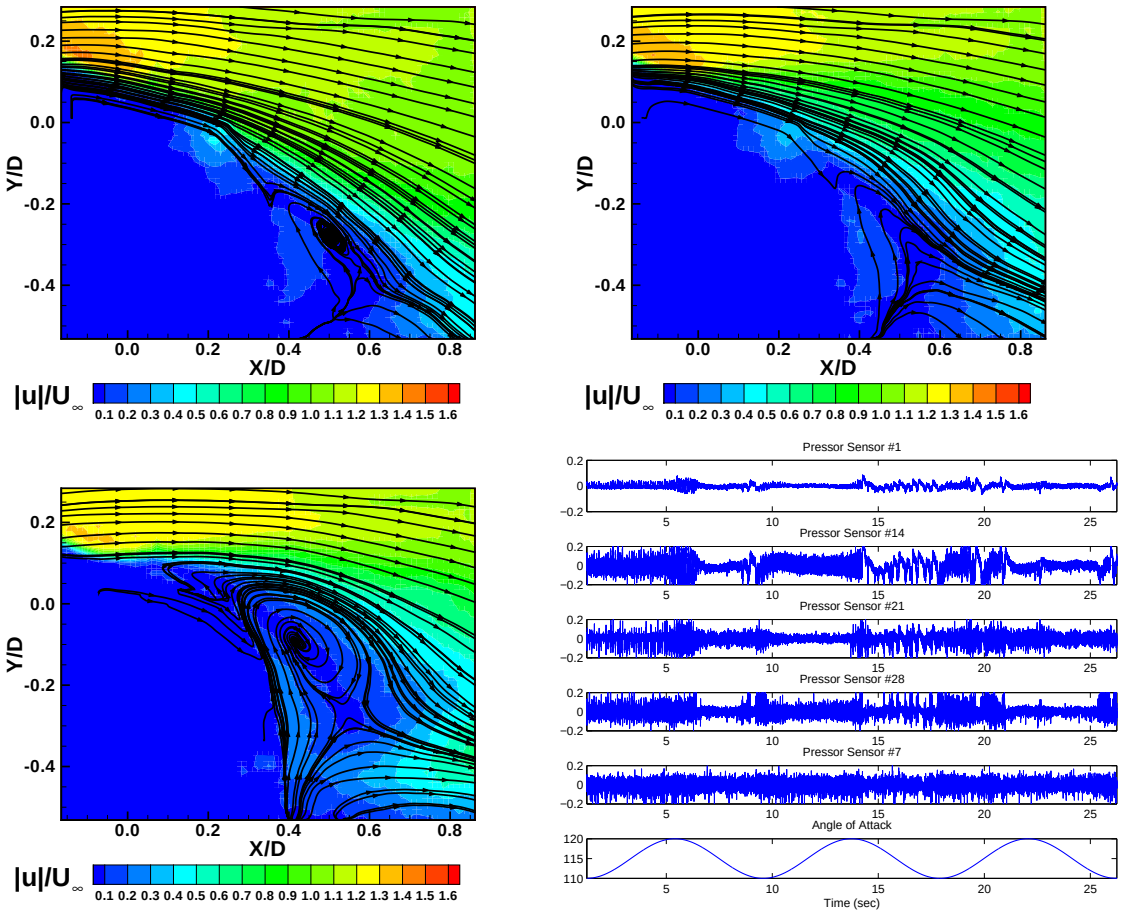

Figure 13. Velocity contours and streamlines in the PIV centerplane from the run with dynamic pitching and closed-loop control (Run 1) at dynamic pitch angles of 115° (increasing) in the top left panel, 120° in the top right panel, and 115° (decreasing) in the bottom left panel. Time histories of five surface pressures on the turret centerline from the dynamic run in the bottom right panel.

Around a Turret Part I: Open Loop Flow Control," AIAA Paper 2008-4216, *4th Flow Control Conference*, Seattle, WA, 2008.

[5]M. Glauser, H. Higuchi, J. Ausseur, J. Pinier, and H. Carlson, "Feedback Control of Separated Flows," AIAA Paper 2004-2521, *2nd AIAA Flow Control Conference*, Portland, OR, 2004.

[6]J. T. Pinier, J. M. Ausseur, M. N. Glauser, and H. Higuchi, "Proportional Closed-Loop Feedback Control of Flow Separation," *AIAA Journal*, **45**, No. 1, 2007, pp. 181-190.

[7]R. D. Wallace, M .Y. Andino, M. Glauser, R. C. Camphouse, R. F. Schmit, and J. H. Myatt, "Flow and Aero-Optics Around a Turret Part II: Surface Pressure Based Proportional Closed Loop Flow Control," AIAA Paper 2008-4217, *4th Flow Control Conference*, Seattle, WA, 2008.

[8]A. J. Smits and J -P. Dussauge, Turbulent Shear Layers in Supersonic Flow, 2nd Edition, Springer 2006.